ISSN 0031-918X, Physics of Metals and Metallography, 2019, Vol. 120, No. 10, pp. 1006–1013. © Pleiades Publishing, Ltd., 2019.
Russian Text © The Author(s), 2019, published in Fizika Metallov i Metallovedenie, 2019, Vol. 120, No. 10, pp. 1101–1108.

STRENGTH AND PLASTICITY

The Microstructure and High-Strain-Rate Superplasticity of the Al–Mg–Ni–Fe–Mn–Cr–Zr Alloy

A. A. Kishchik[a], A. D. Kotov[a], and A. V. Mikhaylovskaya[a, *]

[a] *National University of Science and Technology "MISiS", Moscow, 119049 Russia*

**e-mail: mihaylovskaya@misis.ru*

Received March 7, 2019; revised April 2, 2019; accepted April 22, 2019

Abstract—The microstructure, superplasticity characteristics at a subsolidus temperature (540°C), and the room-temperature mechanical properties of an alloy of the Al–Mg–Ni–Fe–Mn–Cr–Zr system have been investigated using the methods of scanning and transmission electron microscopy and uniaxial tensile tests. The alloy has a bimodal particle-size distribution; it contains eutectic particles of Al_9FeNi with an average size of 0.6 μm; and dispersoids with an average size of 75 nm. The particles of the secondary phases ensure grain size of approximately 4 μm after the recrystallization subsolidus annealing of the cold-rolled sheet. Due to the microsize grain structure, the alloy demonstrates a relative elongation to 500% at a subsolidus temperature in the range of the constant strain rates of 5×10^{-3} to 3×10^{-2} s^{-1}, yield stress 215 MPa, and ultimate strength 330 MPa.

Keywords: aluminum alloy, bimodal structure, grain size, dispersoids, eutectic, superplasticity

DOI: 10.1134/S0031918X19100041

INTRODUCTION

Superplastic forming (SPF) at elevated temperatures makes it possible to obtain articles of complex geometry of enhanced quality made of alloys on different bases [1, 2]. The SPF procedure is based on the phenomenon of superplasticity, i.e., on the opportunity of ensuring stable flow and large elongations without necking because of a high-strain-rate sensitivity of the flow stress [1–3]. The majority of commercial aluminum alloys are superplastic in the range of strain rates of 10^{-4}–10^{-3} s^{-1} with elongations of 200–400%. At a strain rate of 10^{-2} s^{-1}, the elongation does not exceed 150%, and the strain-rate sensitivity of the flow stress is sharply reduced, which does not make it possible to use sheets for forming. To ensure a significant increase in the productivity of superplastic sheet forming and an increase in the economic efficiency of the method, alloys are required that are superplastic at strain rates of 10^{-2} s^{-1} and above [4, 5]. An increase in the rate of superplastic deformation can be achieved via a decrease in the size of recrystallized grains [1–4].

An approach based on the optimization of the heterogeneity of the microstructure [6] is widely applied upon the obtaining of microsize grain structure [6–9]. It is known that fine particles (with a size of <100 nm) provide an efficient retardation of grain growth upon recrystallization [7–12], and that large nondeformable particles of the second phases (>0.3 μm), which are present upon cold deformation, accelerate the formation of nuclei upon subsequent recrystallization [7, 13]. The dispersoids are precipitated from aluminum solid solutions supersaturated by transition and rare-earth elements, e.g., by Mn, Cr, Zr, Sc, or Er [13–21]. According to the Zener theory [22], the smaller the size of the dispersoids and the greater their density, the more significant the effect. To obtain large particles of micron sizes, the alloys can be alloyed by eutectic-forming elements [23–26], which was successfully achieved for guaranteeing high-strain-rate superplasticity in the high-strength alloys of the "nikalin" type [23, 24, 27–29] and a superplastic state in the Al–Cu–Mg alloy of the AA2618 type [30]. A uniform micrograin structure with a grain size of 4 μm and the superplasticity at strain rates to 10^{-1} s^{-1} were achieved by a simple thermomechanical treatment in the Al–Mg–Fe–Ni–Zr–Sc and Al–Zn–Mg–Fe–Ni–Zr–Sc alloys [31–33] due to the formation in their structure of large particles of the Al_9FeNi phase and Al_3(Sc, Zr) dispersoids. Obtaining superplastic alloys without Sc, i.e., with a low cost, remains an urgent task. The principle of the optimization of heterogeneity lies in the basis of the creation of a new alloy Alnovi-U of the Al–Mg–Mn system [34]. Due to the high concentration of manganese (to 1.4 wt %), the particles of phases rich in manganese (eutectic and dispersoids) ensure an enhanced number of recrystallization nuclei and the grain size of 6–8 μm [34] stable at subsolidus temperatures. The alloy shows elongations to 200–250% at enhanced strain rates; its optimum deformation rate is

about 1×10^{-3} s^{-1} [35]. In this work, we have studied the influence of the eutectic-forming elements Fe and Ni and of dispersoid-forming elements Mn and Sr on the microstructure and on the superplasticity characteristics of the Al–5.8Mg alloy with the purpose of obtaining sheets that are superplastic at enhanced deformation rates.

EXPERIMENTAL

We investigated an alloy of composition Al–5.8Mg–0.8Ni–0.6Fe–0.6Mn–0.15Cr–0.1Zr (wt %). The content of silicon was less than 0.02%. The alloy was obtained in a Nabertherm S3 electric furnace in a graphite-chamotte crucible. As the initial materials, aluminum of the A99 grade, magnesium of the Mg95 grade, and preliminarily prepared master alloys Al–10% Fe, Al–20% Ni, Al–10% Mn, Al–5% Zr, and Al–10% Cr were used. The composition of the alloy was analyzed with the aid of the energy-dispersive (EDS) analysis after casting and homogenization annealing. The deviations of the Mg concentration from the specified composition did not exceed 0.2 wt %; those of the other elements, less than 0.05 wt %.

The casting was carried out into a copper water-cooled mold with dimensions of 100 × 40 × 20 mm, which ensured the rate of cooling during casting of about 15 K/s. After casting, the billets were subjected to the following thermomechanical treatment. The homogenization was carried out in two steps: (1) at 430°C for 5 h for the leveling—off of the composition with respect to Mg and precipitation of dispersoids; and (2) at 500°C for 3 h to provide the fragmentation and spheroidization of eutectic particles. The hot and subsequent cold deformations were conducted in a rolling mill with the diameter of rolls of 230 mm. The temperature of the hot rolling was 420 ± 10°C; the degree of deformation was 70%. The cold rolling was conducted to a sheet thickness of 1 mm with a reduction of 80%, after which the sheets were annealed for 20 min at 540°C ($0.97T_m$).

The microstructure was studied with the aid of a Tescan-VEGA3 LMH scanning electron microscope (SEM) equipped with an attachment for the energy-dispersive (X-MAX80, Oxford Instruments) and electron backscatter diffraction (EBSD) analysis. The polished microsections were prepared via mechanical grinding and polishing using a Struers LaboPol machine, and the electrolytic polishing in a chloric-alcohol electrolyte A2 (the production of Struers) at a voltage of 15–20 V. The analysis of the precipitates of second phases was carried out with the aid of a JEOL JEM-2100 transmission electron microscope (TEM). As the objects for the electron-microscopic examination, disks with a diameter of 3 mm were used, which were thinned by mechanical grinding to 0.25 mm, then thinned electrolytically in a jet of the Struers Electrolyte AII in the Struers TenuPol-5 machine at a voltage of 23 V and a temperature of 0 ± 4°C. For the analysis of the grain structure, the polished samples, additionally subjected to oxidizing, were analyzed in the polarized light using a Carl Zeiss Axiovert 200M optical microscope (OM). The oxidation was conducted at a voltage of 10–12 V in an electrolyte consisting of 10% aqueous solution of fluoroboric acid at a temperature of 2–5°C.

The superplasticity characteristics were determined according to the results of uniaxial tensile tests in a Walter Bay LFM100 testing machine. The samples with the size of the cross section $F_0 = 6 \times 1$ mm and with the length of the gage part $L_0 = 14$ mm were cut out parallel to the direction of rolling. The index of the high-strain-rate sensitivity m was determined based on the results of tests with a step-by-step (with steps of 1.5) increase in the deformation rate in the interval of strain rates 5×10^{-5}–8×10^{-2} s^{-1} at a temperature of 540°C. The relative elongation and the value of the flow stress were determined based on the results of tests at the constant values of the rates of deformation equal to 5×10^{-3}, 1×10^{-2}, and 3×10^{-2} s^{-1}. The velocity of motion of the traverse was increased proportional to the increase in the length of the sample to maintain a constant rate of deformation.

The room-temperature mechanical properties were determined using a Zwick-Z250 universal test machine at the rate of deformation equal to 4 mm/min. The samples with dimensions of the gage part of 15 × 6 × 1 mm were cut from the annealed sheet blanks.

RESULTS AND DISCUSSION

The grain size in the cast state varied from 30 to 500 μm and the average was 220 ± 10 μm (Fig. 1a). The microstructure of the alloy after casting (Fig. 1b) and homogenization (Fig. 1c) is represented by particles of phases of crystallization origin, which are located on the periphery of the dendritic cells of the aluminum solid solution. According to the results of the energy-dispersive analysis, it can be concluded that the particles of the crystallization origin are enriched in Fe and Ni (Figs. 1d–1g) and likely belong to the eutectic phase Al_9FeNi [36, 37]. In addition, in the structure of the alloy there is an insignificant amount (volume fraction less than 0.5%) of elongated particles of a phase enriched in Mn and Fe (arrows in Fig. 1g); in all likelihood, these particles belong to the phase $Al_6(Mn, Fe)$, whose crystallization is typical of the alloys of the AA5000 series [38, 39]. The volume fraction of the particles of crystallization origin was 9%; in the cast state, the particles had a size of 0.89 ± 0.11 μm with a form-factor (FF) of 0.69. After the homogenization annealing, the eutectic particles are spheroidized, which follows from an increase of the FF to 0.72; their average size decreases insignificantly (to 0.82 ± 0.09) μm.

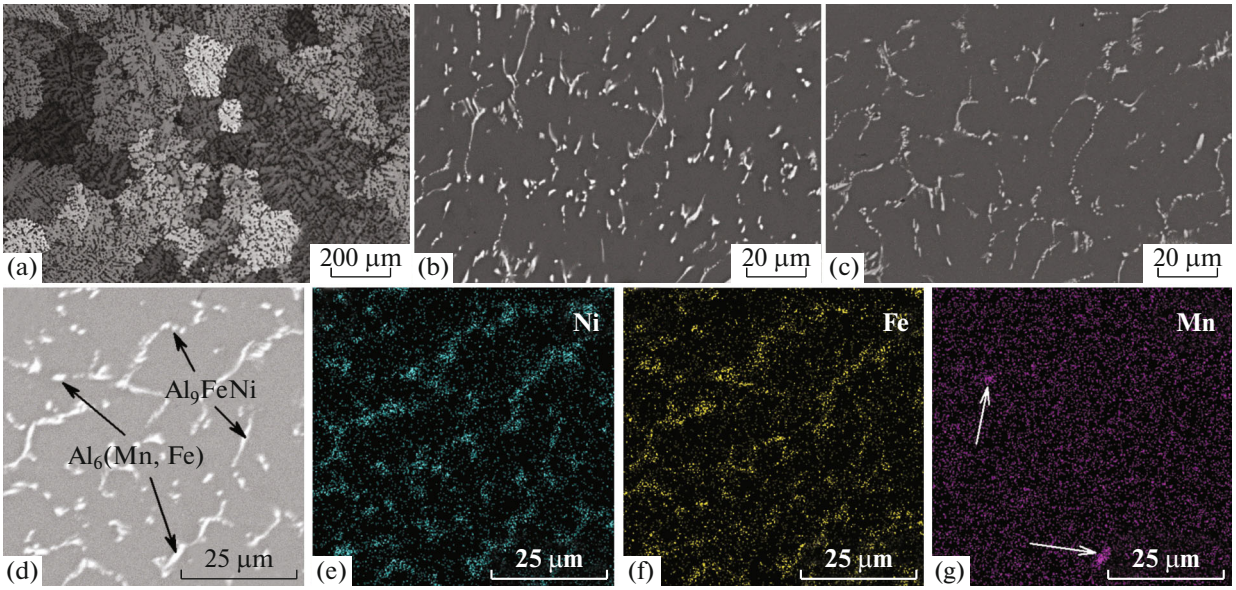

Fig. 1. Structure of the alloy after (a, b) casting and (c, d) homogenization annealing; (e–g) EDS maps of the distribution of the elements Ni (e), Fe (f), and Mn (g) in the region of the microstructure shown in (d); the arrows in (d) indicate the phases of crystallization origin.

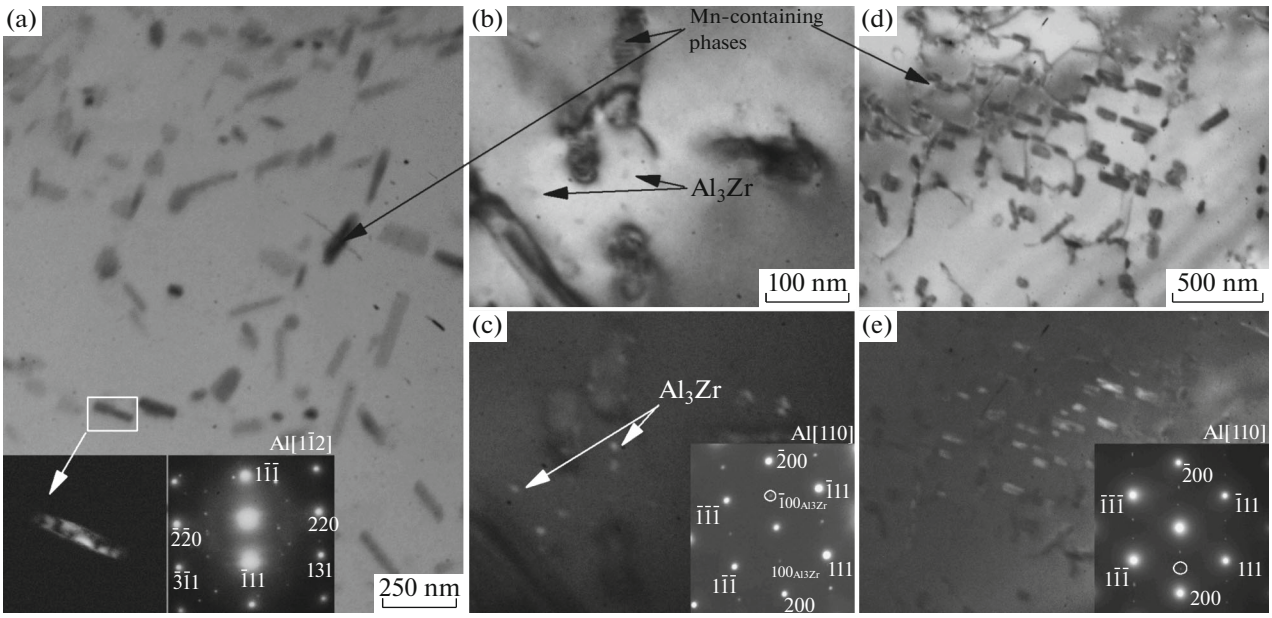

Fig. 2. Particle of dispersoids after the homogenization annealing: (a, b, d) bright-field images (the insets show the dark-field image of the outlined particle and the diffraction pattern); (c, e) the dark field images of the regions (b) and (d), respectively; the insets in (c) and (d) show diffraction patterns; the reflection, in which the dark-field images are obtained, are indicated by small circles.

After the homogenization annealing, dispersoids of two basic types are found in the alloy: (1) elongated particles with a size to 250 nm in the length and to 80 nm in the width (Figs. 2a, 2d, 2e); and (2) compact precipitates of the Al_3Zr phase ($L1_2$ type) with a size to 15 nm (Figs. 2a, 2b). The elongated dispersoids can be completely incoherent to matrix (Fig. 2a, insets); the agglomerates of the elongated dispersoids, like the dispersoids of the Al_3Zr phase, demonstrate an ordered arrangement of the reflections of dispersoids and of the aluminum matrix (Fig. 2e), i.e., the precipitates are identically oriented relative to the matrix, which is

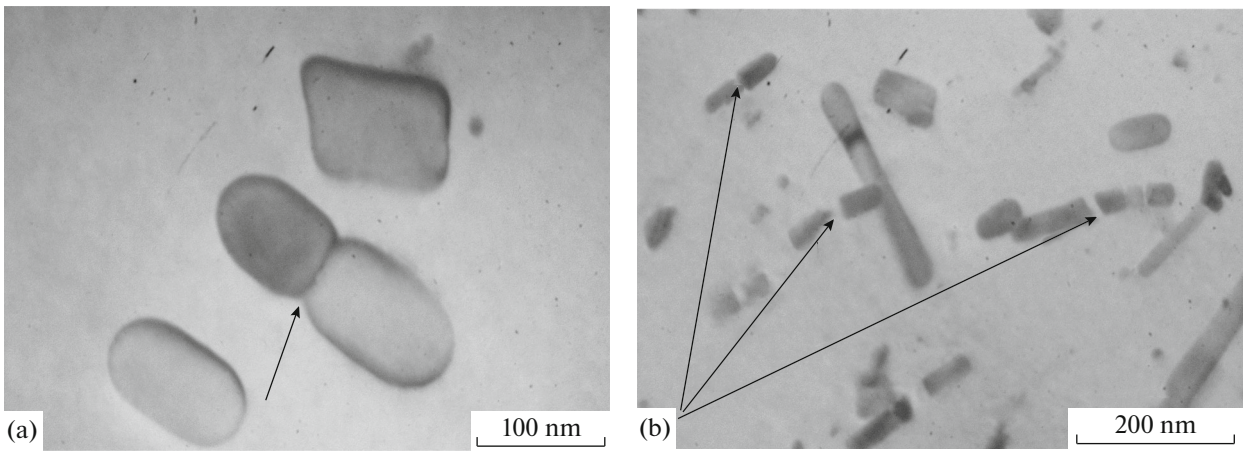

Fig. 3. Particles of dispersoids in the sheets after a thermomechanical treatment: (a) fragmentation of particles; (b) splitting of particles.

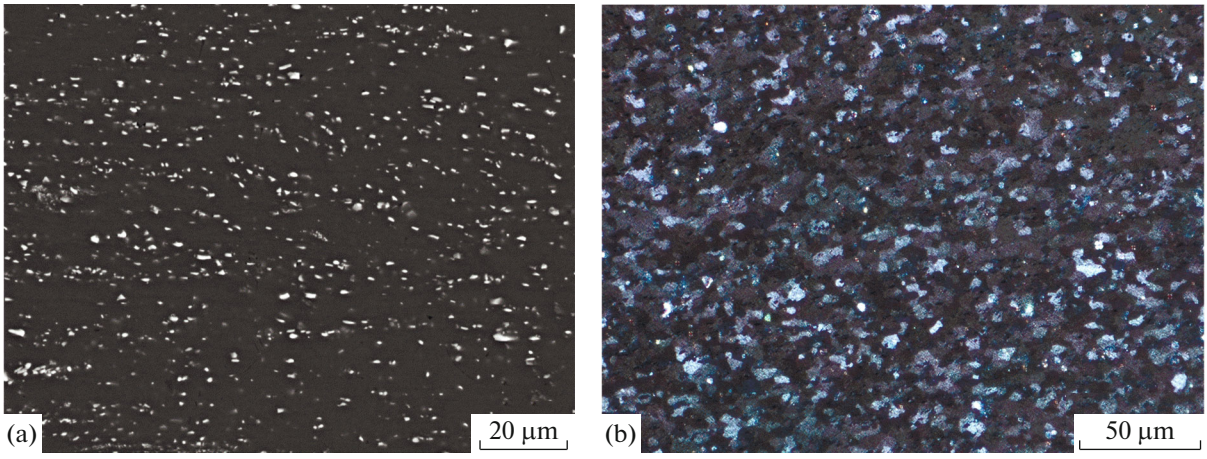

Fig. 4. Microstructure of the alloy after cold deformation (to a sheet thickness of 1 mm) and the grain structure after a 20-min recrystallization annealing at 540°C; (a) SEM; (b) OM, polarized light.

typical of the precipitates coherent to the matrix. The diffraction pattern for the elongated dispersoids differs from the diffraction pattern for the Al_3Zr phase in the case of one zone axis of aluminum [110] (insets in Figs. 2c, 2e). A similar diffraction pattern was observed in the Al–3Mg–1.2Mn–0.3Cr alloy [40]. Judging from the elongated morphology, the dispersoids may belong to the Al_6Mn phase (of which a substitutional dissolution of iron and chromium is typical without a change in the type of the crystal lattice [10, 41]), to its metastable modifications, e.g., to the Al_4Mn phase, or to the α-$Al_{12}Mn_3Si$ phase [41, 42]. It also cannot be excluded that some dispersoids may be related to the ε-$Al_{18}Mg_3Cr_2$ phase [42]. The average size of the manganese-containing dispersoids after thermomechanical treatment was 75 ± 10 nm. The division of particles can occur via their fragmentation trough the formation of constrictions and necks in the bulk of particles (Fig. 3a) by the mechanism similar to the fragmentation of cementite in steels [10, 43]. As a result, the particles become rounded. The size reduction is possible also via mechanical crushing (Fig. 3b) [10].

In the process of obtaining of sheets a change occurs in the parameters of the eutectic particles (Fig. 4a). The particle size in the cold-rolled sheet was 0.57 ± 0.12 μm; the FF increased to 0.82; the volume fraction did not change (9%). The annealing of cold-rolled sheets at a temperature of 540°C for 20 min does not lead to a change in the parameters of the eutectic particles (the average size is 0.58 ± 0.09 μm, FF = 0.82); an almost equiaxed recrystallized structure with

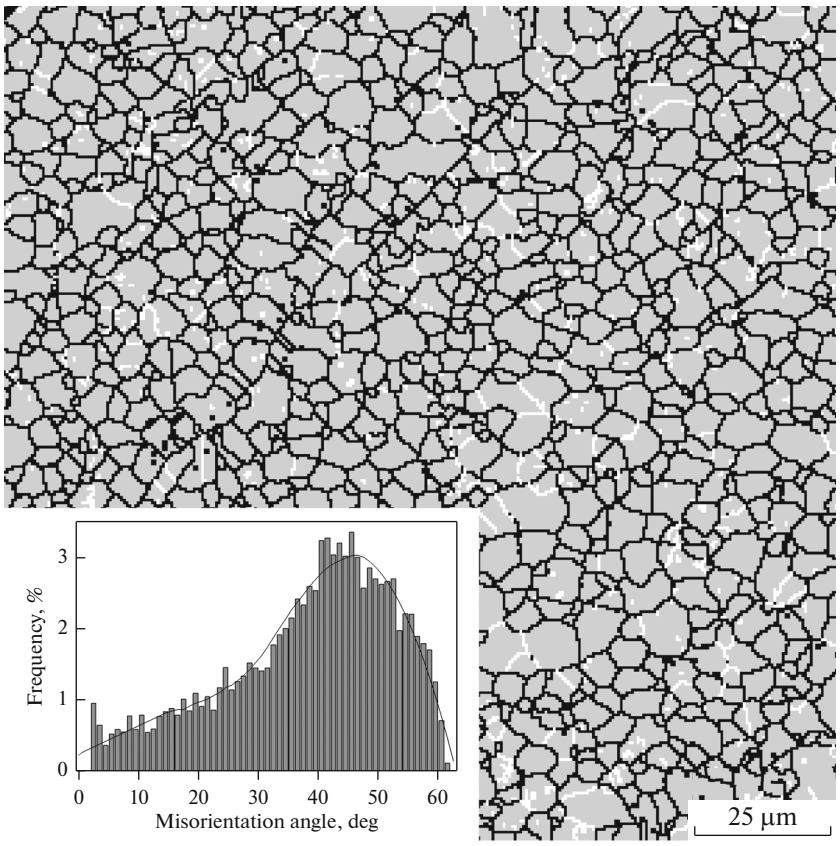

Fig. 5. An EBSD map of grains/subgrains after a 20-min annealing at 540°C (white boundaries correspond to the grain-boundary angle of <15°; black boundaries, to grain-boundary angle of ≥15°); the inset shows a histogram of the distribution of the angles of grain misorientations.

an average grain size of 3.9 ± 0.3 μm is formed (Fig. 4b). The analysis of EBSD maps (Fig. 5) showed that mainly high-angle boundaries (shown in black color in Fig. 5) and ≈10% low-angle boundaries with misorientation of <15° (shown by white color in Fig. 5) are present in the structure of the alloy.

It is known that the Al–Mg-alloys relate to the alloys with a subsolidus superplasticity [44], i.e., manifest the best characteristics near the solidus temperature. According to the results of thermal analysis, the solidus point of the alloy under consideration was 558°C; therefore, to determine the superplasticity indicators we selected the temperature of 540°C ($0.97T_m$). The dependence of the flow stress on the rate of deformation in the logarithmic coordinates has a sigmoidal form (Fig. 6a) typical of the superplastic materials. The maximum values of the coefficient of the strain-rate sensitivity $m = 0.60–0.62$ are observed at the constant strains $(1–2) \times 10^{-2}$ s^{-1}; $m > 0.5$, at the strains of $4 \times 10^{-3}–6 \times 10^{-2}$ s^{-1}. The elongation of the alloy at the constant strain rate of 1×10^{-2} s^{-1} reaches 400%, and the flow stress is 14 MPa. For comparison, in the case of the Alnovi-U alloy intended for the high-strain-rate superplastic forming, the relative elongation at the strain rate 1×10^{-2} s^{-1} does not exceed 270% [34]. The three-fold increase in the strain rate of the investigated alloy (to 3×10^{-2} s^{-1}) leads to an increase in the flow stress to 18 MPa; in this case, the elongation is 280%, which is sufficient for obtaining components of a moderate complexity by the SPF method. For obtaining components of very complex geometry, it is possible to use the rate of deformation 5×10^{-3} s^{-1}, which ensures the relative elongations of more than 500% at the flow stress of 11 MPa.

In the recrystallized state, the alloy has a yield stress equal to 215 ± 5 MPa, the ultimate strength 330 ± 5 MPa, the relative elongation 20 ± 1%. Thus, the alloy demonstrates in the annealed/soft state strength properties at the level of the properties of the AMg6 alloy (AA5085) with a high content of magnesium [45, 46]. The enhanced yield stress of the alloy can be explained by the presence of a microsize grain structure with a grain size of approximately 4 μm.

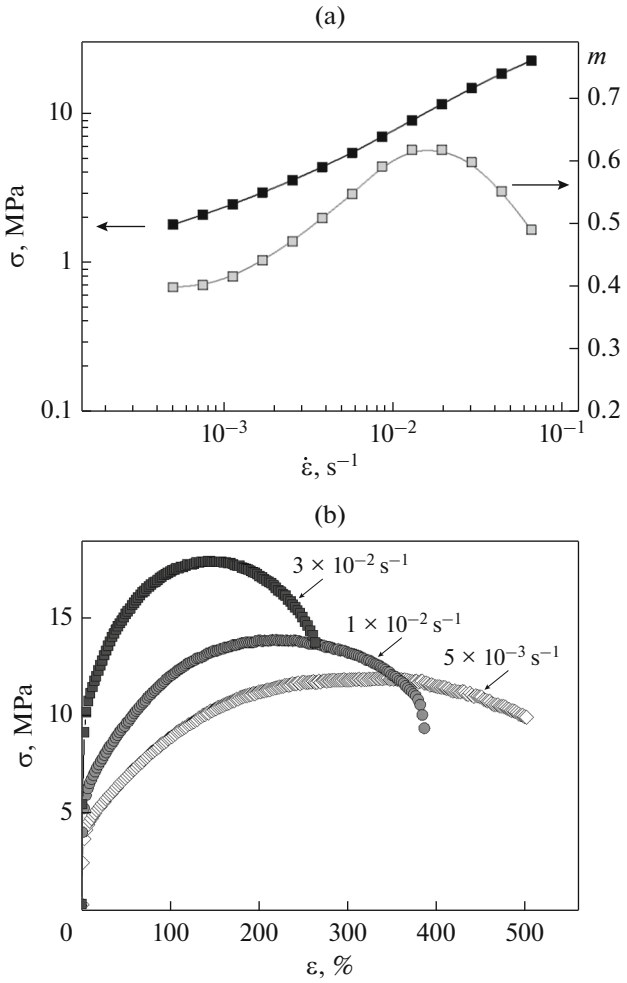

Fig. 6. (a) Dependences of the flow stress σ and of the index of the strain-rate sensitivity *m* on the rate of deformation at a temperature of 540°C; and (b) the relative elongation of the alloy at the temperature of 540°C at different rates of deformation (indicated near the curves).

CONCLUSIONS

(1) Microstructure, room-temperature mechanical properties, grain structure, and characteristics of superplasticity at a temperature of 540°C of an Al–Mg–Fe–Ni–Mn–Cr–Zr alloy have been investigated. It has been shown that upon crystallization of the alloy, eutectic particles are formed with a volume fraction of ≈9%, whose average size decreases from 0.89 to 0.57 μm and the form factor increases from 0.69 to 0.82 in the process of the thermomechanical treatment that includes homogenization annealing, hot rolling, cold rolling, and recrystallization annealing at 540°C (0. 97T_m) for 20 min.

(2) In the process of the homogenization annealing, particles of the Al_3Zr phase ($L1_2$ structure) with dimensions less than 15 nm, and particles of a manganese-containing phase in the form of elongated plates of length to 250 nm are precipitated, which can both have a diffraction pattern typical of the incoherent dispersoids of the Al_6Mn phase with randomly located reflections and demonstrate an ordered arrangement of reflections and identical orientation of the crystal lattice with respect to the lattice of the aluminum matrix. As a result of the deformation treatment, the particles of the Mn-containing phase become fragmented and their average size becomes equal to 75 nm.

(3) After recrystallization annealing at 0.97T_m, the alloy sheets have a grain size of 3.9 μm, a yield stress of 215 MPa, an ultimate strength of 330 MPa, and an elongation of 20%. The microsize grain structure ensures a superplastic state of the alloy with a relative elongation of 270–500% in a range of the constant strains of 5×10^{-3}–3×10^{-2} s^{-1}.

FUNDING

The work was supported by the grant of the Russian Scientific Foundation No. 17-79-20426.

ACKNOWLEDGMENTS

The authors are grateful to Professor V.K. Portnoi (now late) for the discussion of the results of this study.

REFERENCES

1. I. I. Novikov and B. K. Portnoi, *Superplasticity of Alloys with Ultrafine Grain* (Metallurgiya, Moscow, 1981) [in Russian].
2. O. A. Kaibyshev and F. Z. Utyashev, *Superplasticity, Structure Refinement and Processing of Hard-Deforming Alloys* (Nauka, Moscow, 2002) [in Russian].
3. R. A. Vasin and F. U. Enikeev, *Introduction to Superplasticity Mechanics* (Gilem, Ufa, 1998), Part 1 [in Russian].
4. R. Grimes, R. J. Dashwood, and H. M. Flower, "High strain rate superplastic aluminium alloys: The way forward, Mater. Sci. Forum **357–359**, 357–362 (2001).
5. Xiao-guo Wang, Qiu-shu Li, Rui-rui. Wu, Xiao-yuan Zhang, and Liyun Ma, "A review on superplastic formation behavior of Al alloys," Adv. Mater. Sci. Eng., article ID 7606140 (2018). https://doi.org/10.1155/2018/7606140
6. V. K. Portnoi, "The role of heterogeneity optimization in the preparation of ultrafine-grained structure of superplastic alloys," Izv. Vyssh. Uchebn. Zaved., Tsvetn. Metall., No. 1, 93–107 (1985).
7. F. J. Humphreys, "The nucleation of recrystallization at second phase particles in deformed aluminium," Acta Metall. **25**, 1323–1344 (1977).
8. M. V. Markushev, "On the principles of the deformation methods of grain refinement in aluminum alloys to ultrafine size: I. Fine-grained alloys," Phys. Met. Metallogr. **108**, 43–49 (2009).
9. M. V. Markushev, "On the principles of the deformation methods of grain refinement in aluminum alloys to ultrafine size: II. Ultrafine-grained alloys," Phys. Met. Metallogr. **108**, 161–170 (2009).

10. V. K. Portnoy, D. S. Rylov, V. S. Levchenko, and A. V. Mikhaylovskaya, "The influence of chromium on the structure and superplasticity of Al–Mg–Mn alloys," J. Alloys Compd., **581**, 313–317 (2013).
11. A. V. Mikhaylovskaya, O. A. Yakovtseva, I. S. Golovin, A. V. Pozdniakov, and V. K. Portnoy, "Superplastic deformation mechanisms in fine-grained Al–Mg based alloy," Mater. Sci. Eng., A, **627**, 31–41 (2015).
12. A. V. Mikhailovskaya, I. S. Golovin, A. A. Zaitseva, V. K. Portnoi, P. Drottboom, and J. Cifre, "Effect of Mn and Cr additions on kinetics of recrystallization and parameters of grain boundary relaxation of Al–4.9Mg alloy," Phys. Met. Metallogr. **114**, 246–255 (2013).
13. J. A. Wert, N. E. Paton, C. H. Hamilton, and M. W. Mahoney, "Grain refinement in 7475 aluminium by thermomechanical processing," Metall. Trans A **12**, 1267–1276 (1981).
14. P. Yong-yi, Y. Zhi-min, N. Bo, and Z. Li, "Effect of minor Sc and Zr on superplasticity of Al–Mg–Mn alloys," Trans. Nonferrous Met. Soc. China. **17**, 744–750 (2007).
15. Y. Maeng, J. H. Lee, and S. I. Hong, "The effect of transition elements on the superplastic behavior of Al–Mg alloys," Mater. Sci. Eng., A, No. 357, 188–195 (2003).
16. Z. Y. Ma, R. S. Mishra, M. W. Mahoney, and R. Grimes, "High strain rate superplasticity in friction stir processed Al–Mg–Zr alloy," Mater. Sci. Eng., A, **351**, 148–153 (2003).
17. A. Mochugovskiy, A. Mikhaylovskaya, N. Tabachkova, and V. Portnoy, "The mechanism of $L1_2$ phase precipitation, microstructure and tensile properties of Al–Mg–Er–Zr alloy," Mater. Sci. Eng., A **744**, 195–205 (2019).
18. A. V. Pozdniakov, A. A. Aytmagambetov, S. V. Makhov, and V. I. Napalkov, "Effect of impurities of Fe and Si on the structure and strengthening upon annealing of the Al – 0.2% Zr – 0.1% Sc alloys with and without Y additive," Phys. Met. Metallogr. **118**, 479–484 (2017).
19. V. S. Zolotorevskiy, R. I. Dobrojinskaja, V. V. Cheverikin, E. A. Khamnagdaeva, A. V. Pozdniakov, V. S. Levchenko, and E. S. Besogonova, "Strength and substructure of Al–4.7Mg–0.32Mn–0.21Sc–0.09Zr alloy sheets," Phys. Met. Metallogr. **118**, 407–414 (2017).
20. V. S. Zolotorevskiy, R. I. Dobrojinskaja, V. V. Cheverikin, E. A. Khamnagdaeva, A. V. Pozdniakov, V. S. Levchenko, and E. S. Besogonova, "Evolution of structure and mechanical properties of Al–4.7Mg–0.32Mn–0.21Sc–0.09Zr alloy sheets after accumulated deformation during rolling," Phys. Met. Metallogr. **117**, 1163–1169 (2016).
21. O. S. Sitdikov, E. V. Avtokratova, O. E. Mukhametdinova, R. N. Garipova, and M. V. Markushev, "Effect of the size of Al_3(Sc, Zr) precipitates on the structure of multi-directionally isothermally forged Al–Mg–Sc–Zr alloy," Phys. Met. Metallogr. **118**, 1215–1224 (2017).
22. E. Nes, N. Ryum, and O. Hunderi, "On the Zener drag," Acta Metall. **33**, 11–22 (1985).
23. N. A. Belov, "Quantitative phase analysis of the Al–Zn–Mg–Cu–Ni phase diagram in the region of compositions of high-strength nickalines," Russ. J. Non-Ferrous Met. **51**, 243–249 (2010).
24. P. K. Shurkin, N. A. Belov, T. K. Akopyan, A. N. Alabin, A. S. Aleshchenko, and N. N. Avxentieva, "Formation of the structure of thin-sheet rolled product from a high-strength sparingly alloyed aluminum alloy "nikalin"," Phys. Met. Metallogr. **118**, 896–904 (2017).
25. T. K. Akopyan, A. S. Aleshchenko, N. A. Belov, and S. P. Galkin, "Effect of Radial–shear rolling on the formation of structure and mechanical properties of Al–Ni and Al–Ca aluminum–matrix composite alloys of eutectic type," Phys. Met. Metallogr. **119**, 241–250 (2018).
26. A. V. Mikhaylovskaya, M. A. Ryazantseva, and V. K. Portnoy, "Effect of eutectic particles on the grain size control and the superplasticity of aluminium alloys," Mater. Sci. Eng., A **528**, 7306–7309 (2011).
27. A. D. Kotov, A. V. Mikhaylovskaya, and V. K. Portnoy, "Effect of the solid-solution composition on the superplasticity characteristics of Al–Zn–Mg–Cu–Ni–Zr alloys," Phys. Met. Metallogr. **115**, 730–735 (2014).
28. A. D. Kotov, A. V. Mikhaylovskaya, M. S. Kishchik, A. A. Tsarkov, S. A. Aksenov, and V. K. Portnoy, "Superplasticity of high-strength Al-based alloys produced by thermomechanical treatment," J. Alloys Compd. **688**, 336–344 (2016).
29. A. D. Kotov, A. V. Mikhaylovskaya, A. A. Borisov, O. A. Yakovtseva, and V. K. Portnoy, "High-strain-rate superplasticity of the Al–Zn–Mg–Cu alloys with Fe and Ni additions," Phys. Met. Metallogr. **118**, 913–921 (2017).
30. A. D. Kotov, A. V. Mikhaylovskaya, I. S. Golovin, and V. K. Portnoy, "Fine-grained structure and superplasticity of Al–Cu–Mg–Fe–Ni alloys," Mater. Sci. Forum **735**, 55–60 (2013).
31. A. Kishchik, A. Mikhaylovskaya, A. Kotov, and V. Portnoy, "Effect of homogenization treatment on superplastic properties of aluminum based alloy with minor Zr and Sc additions," Defect Diffus. Forum **385**, 84–90 (2018).
32. A. V. Mikhaylovskaya, O. A. Yakovtseva, V. V. Cheverikin, A. D. Kotov, and V. K. Portnoy, "Superplastic behaviour of Al–Mg–Zn–Zr–Sc-based alloys at high strain rates," Mater. Sci. Eng., A **659**, 225–233 (2016).
33. A. A. Kishchik, A. V. Mikhaylovskaya, A. D. Kotov, O. V. Rofman, and V. K. Portnoy, "Al–Mg–Fe–Ni-based alloy for high strain rate superplastic forming," Mater. Sci. Eng., A **718**, 190–197 (2018).
34. T. Kudo, A. Goto, and K. Saito, "High Strain Rate Blow Formability of Newly Developed Al–Mg–High–Mn Alloy," Furukawa-Sky Rev., No. 9, 11–17 (2013).
35. D. Sorgente and L. Tricarico, "Characterization of a superplastic aluminium alloy ALNOVI-through free inflation tests and inverse analysis," Int. J. Mater. Form., No. 7, 79–87 (2014).
36. L. F. Mondolfo, *Aluminum Alloys: Structure and Properties* (Oxford, Butterworths, 1976).
37. M. Glazoff, A. Khvan, V. Zolotorevsky, N. Belov, and A. Dinsdale, *Casting Aluminum Alloys, their Physical and Mechanical Metallurgy, 2nd Edition* (Elsevier, 2018).

38. O. Engler, Z. Liu, and K. Kuhnke, "Control of second-phase particles in the Al–Mg–Mn alloy AA 5083," J. Alloys Compd. **689**, 998–1010 (2016).

39. O. Engler, Z. Liu, and K. Kuhnke, "Impact of homogenization on particles in the Al–Mg–Mn alloy AA 5454—Experiment and simulation," J. Alloys Compd. **560**, 111–122 (2013).

40. A. V. Mikhaylovskaya, V. K. Portnoy, A. G. Mochugovskiy, M. Yu. Zadorozhnyy, N. Yu. Tabachkova, and I. S. Golovin, "Effect of homogenisation treatment on precipitation, recrystallisation and properties of Al–3% Mg–TM alloys (TM = Mn, Cr, Zr)," Mater. Des. **109**, 197–208 (2016).

41. O. Engler, K. Kuhnke, K. Westphal, and J. Hasenclever, "Impact of chromium on the microchemistry evolution during solidification and homogenization of the Al–Mg alloy AA 5052," J. Alloys Compd. **744**, 561–573 (2018).

42. Y. J. Li and L. Arnberg, "Quantitative study on the precipitation behavior of dispersoids in DC-cast AA3003 alloy during heating and homogenization," Acta Mater. **51**, 3415–3428 (2003).

43. L. Zhou, G. Liu, X. L. Ma, and K. Lu, "Strain-induced refinement in a steel with spheroidal cementite subjected to surface mechanical attrition treatment," Acta Mater. **56**, 78–87 (2008).

44. I. I. Novikov, V. K. Portnoy, V. S. Levchenko, and A. O. Nikiforov, "Subsolidus superplasticity of aluminium alloys," Mater. Sci. Forum **243–245**, 463–468 (1997).

45. M. V. Markushev and M. Yu. Murashkin, "Strength and crack resistance of commercial aluminum alloys 1560 and 5083 of the Al–Mg–Mn system after severe plastic deformation via angular pressing," Phys. Met. Metallogr. **98**, 221–231 (2004).

46. E. Romhanji, M. Popovic, D. Glisic, and V. Milenkovic, "Formability of a high-strength Al–Mg6.8 type alloy sheet," J. Mater. Sci. **33**, 1037–1042 (1998).

Translated by S. Gorin